Structural Basis for Integration of GluD Receptors within Synaptic Organizer Complexes

Jonathan Elegheert[1], **Wataru Kakegawa**[2], **Jordan E. Clay**[1], **Natalie F. Shanks**[3], **Ester Behiels**[1], **Keiko Matsuda**[2], **Kazuhisa Kohda**[2], **Eriko Miura**[2], **Maxim Rossmann**[4], **Nikolaos Mitakidis**[1], **Junko Motohashi**[2], **Veronica T. Chang**[1], **Christian Siebold**[1], **Ingo H. Greger**[4], **Terunaga Nakagawa**[3,†], **Michisuke Yuzaki**[2,†,*], and **A. Radu Aricescu**[1,†,*]

[1]Division of Structural Biology, Wellcome Trust Centre for Human Genetics, University of Oxford, Roosevelt Drive, Oxford, OX3 7BN, UK

[2]Department of Physiology, Keio University School of Medicine, 35 Shinanomachi, Shinjuku-ku, Tokyo, 160-8582, Japan

[3]Department of Molecular Physiology and Biophysics, School of Medicine, Vanderbilt University, Nashville, TN, 37232-0615, USA

[4]Neurobiology Division, MRC Laboratory of Molecular Biology, Francis Crick Avenue, Cambridge, CB2 0QH, UK

Abstract

Ionotropic glutamate receptor family members (iGluRs) are integrated into supramolecular complexes that modulate their location and function at excitatory synapses. However, a lack of structural information beyond isolated receptors or fragments thereof currently limits the mechanistic understanding of physiological iGluR signaling. Here, we report structural and functional analyses of the prototypical molecular bridge linking post-synaptic iGluR δ2 (GluD2) and pre-synaptic β-neurexin-1 (β-NRX1) via Cbln1, a C1q-like synaptic organizer. We show how Cbln1 hexamers "anchor" GluD2 amino-terminal domain dimers to monomeric β-NRX1. This arrangement promotes synaptogenesis, and is essential for D-Serine-dependent GluD2 signaling *in vivo*, underlying long-term depression of cerebellar parallel fiber-Purkinje cell (PF-PC) synapses and motor coordination in developing mice. These results lead to a model where protein and small-molecule ligands synergistically control synaptic iGluR function.

Excitatory neurotransmission in the vertebrate central nervous system is largely mediated by the iGluR family members, classified as AMPA (GluA1-4), NMDA (GluN1, GluN2A-D, GluN3A-B), Kainate (GluK1-5) and Delta (GluD1-2) subtypes (1). All iGluRs are assembled from four modular subunits, each displaying extracellular amino-terminal and ligand binding domains (ATD and LBD), a transmembrane domain (TMD) lining a central ion channel pore, and a cytoplasmic carboxy-terminal domain (CTD) (2–6). Binding of agonist molecules to the LBDs of GluA, GluN and GluK receptors (typically glutamate, but also glycine or D-Serine for GluN subtypes) drives opening of the cation-conductive ion

[*]Correspondence to: radu@strubi.ox.ac.uk (A.R.A); myuzaki@a5.keio.jp (M.Y.).
[†]Co-senior author

channel and neuronal membrane depolarization (1). Furthermore, all iGluRs appear to initiate post-synaptic signaling through non-ionotropic mechanisms, a process better understood for NMDA and Delta receptor subtypes (7–15).

In addition to their signaling function, mediated by excitatory amino acids, iGluRs are implicated in synaptogenesis (16–20). The membrane-distal position of iGluR ATDs makes them readily accessible to other proteins populating the synaptic cleft. In this context, the GluD subfamily of iGluRs are the best studied. Cbln1, a soluble synaptic organizer molecule belonging to the C1q/TNFα superfamily (21), directly binds the GluD1 and GluD2 ATDs (16, 18, 22, 23). Cbln1 also interacts with pre-synaptic membrane-tethered neurexins (NRXs) (18), establishing "molecular bridges" that span the cleft to facilitate bi-directional synaptic differentiation (16, 18). Despite their importance, the architecture of supramolecular GluD assemblies and the mechanisms by which they support integration of the dual synaptogenic and metabotropic signaling functions have remained unknown. We sought to address these questions by structurally investigating the β-NRX1–Cbln1–GluD2 trans-synaptic triad.

As a first step towards solving a Cbln–GluD complex, we solved high-resolution crystal structures of (i) free human GluD2 ($GluD2_{ATD}$, 1.75 Å) and mouse GluD1 ($GluD1_{ATD}$, 2.30 Å) ATD dimers, and (ii) free nearly full-length human Cbln1 ($Cbln1^{VRSG}$, 2.80 and 7.00 Å) and the obligate Cbln1 globular domain trimer (with a C1q-like fold, $Cbln1_{C1q}$, 2.35 Å) (fig. S1-S4, table S1 and (24)). Using Surface Plasmon Resonance (SPR), we found that avidity governs the full-length Cbln1–GluD2 ($Cbln1_{FL}$–$GluD2_{FL}$) complex formation, resulting in a nM-range apparent affinity ($K_{D,app}$ ~ 125 nM) (fig. S5 and (24)). Molecular dissection of the complex into individual components revealed that the Cbln1 C1q-like trimer is the minimal unit needed for interaction with $GluD2_{ATD}$, with an affinity in the high μM-range (fig. S5-S6 and (24)). Attempts at co-crystallizing a Cbln1–$GluD2_{ATD}$ complex were hampered by the propensity of both components to crystallize separately. We consequently designed a construct that combines a fused $Cbln1_{C1q}$ trimer with $GluD2_{ATD}$ into one continuous polypeptide chain, linked by a 30-residue flexible Gly-Gly-Ser ($(G_2S)_{10}$) spacer (Fig. 1A, fig. S7-S8 and (24)). We validated the mass and monodispersity of the $Cbln1_{C1q}$–$GluD2_{ATD}$ chimera using Multi-angle Light Scattering (MALS) and negative-staining single particle EM (fig. S8 and (24)).

We determined the crystal structure of the $Cbln1_{C1q}$–$GluD2_{ATD}$ complex at 3.10 Å (Fig. 1B, fig. S8 and table S1). $Cbln1_{C1q}$ sits on top of the membrane-distal face of the $GluD2_{ATD}$ in an inward tilted orientation and breaks its threefold symmetry to engage an ATD monomer with a total buried surface area (BSA) of 873 Å^2 (Fig. 1C). The arrangement of both $Cbln1_{C1q}$ trimers suggests the position of the putative Cbln1 N-terminal "Cys-rich region" (CRR, not present in the chimeric construct) that links two $Cbln1_{C1q}$ trimers into the hexameric $Cbln1_{FL}$ (Fig. 1B, fig. S4 and (25)). The distance between the calculated centers of mass of both trimers is 70 Å, in good agreement with the corresponding distances in two crystal structures of free $Cbln1^{VRSG}$ (77 and 79 Å, respectively, fig. S9). The tilted vs. linear arrangement of the C1q trimers in the three structures suggests their intrinsic hinge movement relative to the CRR (fig. S9), consistent with the single-particle EM analysis (Fig. 1D and fig. S10). The $Cbln1_{C1q}$–$GluD2_{ATD}$ structure however indicates that binding of

GluD2 constrains the $Cbln1_{C1q}$ domain orientation. Single-particle EM class averages of free $Cbln1_{FL}$ indicated the CRR as a globular structure linking two Cbln1 C1q trimers (Fig. 1D, fig. S10 and (24)).

In the $Cbln1_{C1q}$–$GluD2_{ATD}$ crystal lattice, $GluD2_{ATD}$ forms the same N-shaped tetrameric "AB–CD" arrangement (Fig. 2A) previously observed in the full-length GluA2 and GluK2 structures (5, 26) and in structures of isolated GluA2 (27, 28) and GluK6 (29) ATDs. Cα-atom superposition of $GluA2_{CRYST}$ (5) and GluD2 ATD tetramers yields an r.m.s.d. of 5.6 Å over 635 positions when aligning B–D dimers, and 7.3 Å over 695 positions when aligning A–C dimers (Fig. 2B). This AB–CD ATD arrangement is, as in $GluA2_{CRYST}$, stabilized by two-fold symmetrical contacts between the D–B monomers (666 $Å^2$ BSA), and consists of numerous putative salt bridges and hydrogen bonds as well as two potential calcium atoms (fig. S11 and (24)). Alignment of the $Cbln1_{C1q}$–$GluD2_{ATD}$ complex to the full $GluA2_{CRYST}$, using the B–D ATD dimer as reference, illustrates how one Cbln1 hexamer, binding to each ATD dimer, extends the outward-tapering, vertical Y-shape of the iGluR. The height of this arrangement (~17 nm) fits within the typical width of the PF-PC synaptic cleft (~20 nm) (Fig. 2C).

We then investigated how Cbln1 links GluD2 to pre-synaptic β-NRX1. The extracellular part of the single-span membrane-tethered β-NRX1 consists of a single LNS (laminin, neurexin, sex-hormone-binding globulin) domain, LNS6, of known structure (30). Insertion of the 30-residue "spliced sequence #4" (SS4) into $β-NRX1_{LNS6}$ via alternative splicing, to yield β-NRX1(+4), is required for Cbln1 binding (18). Using Isothermal Titration Calorimetry (ITC), we measured that one hexameric Cbln1 and one monomeric β-NRX1(+4) bind with high-affinity (K_D = 43.5 ± 4.4 nM), and that the Cbln1 CRR and β-NRX1 SS4 mediate all binding (fig. S12). Surprisingly, the 1-to-1 stoichiometry indicates that the two-fold Cbln1 symmetry is broken in β-NRX1(+4)–$Cbln1_{FL}$. Single-particle negative-stain EM class averages of β-NRX1(+4)–$Cbln1_{FL}$ confirm this stoichiometry and confirm that the Cbln1 CRR is the β-NRX1(+4) binding platform (Fig. 2D, fig. S10 and (24)). Together, our structural analyses allow us to propose an overall model for the β-NRX1–Cbln1–GluD2 triad that features symmetry mismatches in both binary complex interfaces (Fig. 2E).

$Cbln1_{C1q}$ binds $GluD2_{ATD}$ at the membrane-distal ends of α-helices 1, 2, 3, 9 and 10 of the R1 lobe and the "flap" loop, an extended, structurally conserved segment that links α-helices 9 and 10 and folds back onto the top of the ATD. Cbln1 interface residues are contributed by loops AA' (Ser^{69}-Ser^{75}), CD (Tyr^{122}-Thr^{126}), EF ($Glys^{144}$-Arg^{150}) and GH (Gly^{174}-Lys^{181}) from one C1q subunit (Fig. 3A). Cbln1 loops EF and CD rearrange upon binding the relatively flat top of $GluD2_{ATD}$, which remains largely unchanged between free and Cbln1-bound states (overall Cα-atom r.m.s.d. of 0.5 Å over 336 positions) (Fig. 3A).

Cbln1 Tyr^{122} forms the central interaction hotspot; it is oriented by GluD2 Glu^{61} and Thr^{60} and buried in a small hydrophobic pocket formed by GluD2 Ile^{26}, Ile^{27}, Leu^{58}, Leu^{342} and Trp^{347} (fig. S13). At the periphery, Asp^{24}, the first residue of the mature GluD2 chain, is locked into an extended putative hydrogen-bonding network by Cbln1 residues Thr^{70}, Asn^{71} and His^{72} of loop AA', and Lys^{181} of loop GH. Cbln1 Arg^{150} and Asp^{147} on loop EF engage in putative charged interactions with GluD2 Glu^{61} and Arg^{345}, respectively (fig. S13).

Sequence conservation analysis indicates that the flap loop interface residues of $GluD1/2_{ATD}$, and the loop-based interface residues in the Cbln family (Cbln1-Cbln4) are highly conserved in vertebrates (fig. S14).

We performed single-position alanine-scanning mutagenesis on 15 contiguous GluD2 interface residues to validate the $Cbln1_{C1q}$–$GluD2_{ATD}$ binding mode. D24A, S25A, I26A, E61A, L342A, R345A, H348A and S352A cluster into the center of the observed interaction interface and showed reduced binding to Cbln1 in an avidity-enhanced SPR setup. Seven peripheral mutations maintained binding: T60A, E343A, D344A, K346A, S349A, M350A and Q364A (Fig. 3B, 3C and fig. S15). Furthermore, the $Cbln1_{FL}$, $Cbln1^{C34S,C38S}$ (lacking the CRR) and $Cbln1_{C1q}$ variants containing the Y122A, R124A and D147A interface mutations lost all binding to $GluD2_{ATD}$ (fig. S16).

The expression pattern of GluD2, specifically confined to PF-PC synapses in the cerebellar cortex (31), and the availability of well characterized *Grid2*-null (GluD2-deficient) and *Cbln1*-null mice, offered us the opportunity to validate and mechanistically interrogate structural models in a series of functional assays, from cell culture to *in vivo*. Guided by the $Cbln1_{C1q}$– $GluD2_{ATD}$ structure, we designed a number of GluD2 mutants that target distinct structural features of the receptor to gauge their effect on the two well-established major functions of GluD2 signaling: (i) PF-PC synapse formation and (ii) induction of long-term depression (LTD) of synaptic transmission (8, 31). $GluD2^{D24A,I26A,E61A,R345A}$ combines four Ala-mutations that abolish Cbln1 binding (Fig. 3B and fig. S17). $GluD2^{E343A,K346A,S349A,M350A}$ combines four Ala-mutations that maintain Cbln1 binding but are immediately adjacent to the binding hotspot (Fig. 3B and fig. S17). $GluD2^{F76D}$ contains monomerised ATDs (fig. S6); this mutation was specifically designed to disrupt the N-shaped ATD-layer, native $Cbln1_{FL}$–$GluD2_{ATD}$ binding geometry and overall Y-shape of GluD2 (Fig. 2C), while maintaining the $Cbln1_{C1q}$ binding platform (Fig. 3A). Finally, $GluD2^{ATD-LBD\_GLYCAN\_WEDGE}$ contains a ten-residue glycosylated linker (ELSNGTDGAS in single-letter amino acid code) inserted between the ATD and LBD layers in order to space them apart and disrupt potential mechanical ATD-LBD coupling (fig. S17 and (24)).

The effect of the glycan wedge (GW) on ATD-LBD coupling was tested by introducing the Ala654Thr mutation ("Lurcher" (Lc), located in TM helix M3) into GluD2 to render the channel constitutively open (fig. S18). Application of the LBD agonist D-Serine (D-Ser) inhibited the Lc current in a dose-dependent manner, as expected (32). However, the half-maximal inhibitory concentration (IC_{50}) was ~1.5-fold higher in $GluD2^{GW/Lc}$ compared to $GluD2^{WT/Lc}$, indicating that separation of ATD and LBD by the glycan wedge impaired the ability of the LBD to induce pore closure (fig. S18).

We set up a heterologous hemi-synapse formation assay in which HEK 293T cells expressing these mutants were co-cultured with isolated wild-type mouse cerebellar granule cells (GCs) (Fig. 3D and fig. S17). Consistent with our mutagenesis data, cells expressing $GluD2^{D24A,I26A,E61A,R345A}$ accumulated no GC axon terminals whereas cells expressing $GluD2^{E343A,K346A,S349A,M350A}$ did so normally. Cells expressing $GluD2^{F76D}$ showed intermediate GC axon terminal accumulation, suggesting that a disrupted ATD dimerization interface still allows synapse-spanning interactions to a certain extent. The

GluD2$^{\text{ATD-LBD\_GLYCAN\_WEDGE}}$ mutant showed normal GC axon terminal accumulation, in line with the Cbln1$_{\text{C1q}}$–GluD2$_{\text{ATD}}$ complex interface, as well as receptor geometry, being intact.

We back-expressed GluD2$^{\text{WT}}$ and the GluD2 mutants using recombinant Sindbis virus into the cerebellum of adult (> P30) *Grid2*-null mice that typically display a marked (~40%) reduction of PF-PC synapse number (31). Immunohistochemical (IHC) analysis of ultrathin sections using gold-conjugated anti-GluD2 antibodies detected that all mutants reached the PC post-synaptic density (PSD) (fig. S19). We counted the number of PF-PC synapses in the EM micrographs; the proportion of contacted synapses for GluD2$^{\text{E343A,K346A,S349A,M350A}}$ and GluD2$^{\text{ATD-LBD\_GLYCAN\_WEDGE}}$ was comparable to GluD2$^{\text{WT}}$. GluD2$^{\text{D24A,I26A,E61A,R345A}}$ and GluD2$^{\text{F76D}}$ however failed to robustly induce PF-PC contacts (Fig. 3E and fig. S19). Thus, disruption of the Cbln1–GluD2 interface and binding geometry attenuates rapid induction of PF-PC synapses.

Cerebellar LTD is caused by activity-induced endocytosis of postsynaptic AMPA receptors in PC dendrites (33). GluD2 signaling via the CTD is absolutely required for LTD induction independent of PF synapse formation; LTD is impaired even when the PF synapse number is restored by reintroduction of GluD2 lacking the CTD in *Grid*-null mice (34). D-Ser binds and closes the LBD of GluD2 (fig. S18 and (32)) to enhance LTD induction via the CTD of GluD2 (8). Interestingly, application of exogenous D-Ser (200 μM for 10 min) reduced PF-evoked excitatory postsynaptic currents (PF-EPSCs) in mature wild-type, but not in *Cbln1*-null PCs, in the presence of NMDA receptor blockers to prevent co-activation of NMDA receptors (fig. S20). Endogenous D-Ser is released at PF-PC synapses from neighboring Bergmann glia by burst stimulation (BS) of PFs in immature cerebellar slices (8). Indeed, conjunctive BS and direct PC depolarization (BS/ V) (Fig. 4A) induced a robust LTD in wild-type, but not in *Cbln1*-null or *Grid2*-null PCs in the presence of NMDA receptor blockers (fig. S20). These results indicate that GluD2 requires the presence of Cbln1 in order to respond to exo- or endogenous D-Ser and trigger AMPA receptor endocytosis.

We examined whether the structure-guided GluD2 mutants are able to support D-Ser-dependent LTD at PF-PC synapses. BS/ V induced LTD in immature *Grid2*-null PCs expressing GluD2$^{\text{WT}}$ and GluD2$^{\text{E343A,K346A,S349A,M350A}}$, but not GluD2$^{\text{D24A,I26A,E61A,R345A}}$, GluD2$^{\text{F76D}}$ or GluD2$^{\text{ATD-LBD\_GLYCAN\_WEDGE}}$ (Fig. 4B, fig. S21 and (24)). Thus, anchoring by Cbln1, stable ATD dimer formation and ATD-LBD coupling are all required for GluD2 to mediate the D-Ser-dependent LTD signals.

To relate our findings to cerebellar function *in vivo*, we subjected immature *Grid2*-null mice virally expressing GluD2$^{\text{WT}}$ and the structure-guided GluD2 mutants to an accelerating (4 to 40 r.p.m. in 5 min) rotor-rod test. Conventional cerebellum-dependent learning tasks such as eye blink-conditioning cannot be used in immature mice, when D-Ser is still present. Motor coordination was recovered following expression of GluD2$^{\text{WT}}$, GluD2$^{\text{E343A,K346A,S349A,M350A}}$ and GluD2$^{\text{ATD-LBD\_GLYCAN\_WEDGE}}$, but not of GluD2$^{\text{D24A,I26A,E61A,R345A}}$ or GluD2$^{\text{F76D}}$ (fig. S22). These results reflect our PF-PC synapse formation data and suggest that the interface and geometry of the Cbln1–GluD2

complex we describe is crucial for restoration of PF-PC cerebellar circuitry and motor-related performance.

Our results provide a molecular framework for the large body of studies on the β-NRX1–Cbln1–GluD2 trans-synaptic signaling system, and suggest a three-step model for GluD2 signaling activation. Cbln1 is secreted from cerebellar GCs through yet unidentified mechanisms and remains associated with β-NRX1 on the surface of GC axons (Fig. 4C, Step I) (35). When cerebellar GC axons encounter PC dendritic spines, the β-NRX1–Cbln1 complex "hooks" GluD2, via avidity-enhanced $Cbln1_{C1q}$–$GluD2_{ATD}$ interactions, in a trans-synaptic complex (Fig. 4C, Step II). The biological importance of the binding avidity most likely lies in improving the probability for molecular recruitment of GluD2 by β-NRX1–Cbln1 at PF-PC synapses, given the weak affinity between individual Cbln1 and GluD2 domains. It is however unclear whether GluD2 is fully occupied at any given time point. Finally, agonist binding triggers a conformational change of the GluD2 LBD which is transmitted to the transmembrane domain to initiate downstream signaling (9) resulting in AMPA receptor endocytosis and LTD (8, 9) (Fig. 4C, Step III).

Recent structures of isolated full-length GluA and GluK receptors in different functional states have established that iGluR gating is accompanied by complex ATD-LBD relative motions (26, 36, 37). Furthermore, desensitization of GluA receptors results in a marked conformational variability in the ATD layer (4, 26, 36). Similar motions might, in principle, be possible in GluD receptors, considering their overall structural and sequence homology to GluA and GluK family members. However, we propose that, in a trans-synaptic context, anchoring of GluD to the β-NRX1(+4)–Cbln1 complex will limit or prevent large-scale motions of the ATD layer. As a result, the force generated by LBD closure, driving the overall receptor contraction, is likely to transfer predominantly towards the post-synaptic membrane. Since most, if not all, iGluR family members are anchored to synaptic cleft proteins via their ATDs (16–20), it is conceivable that their range of motions may also differ from those currently described in isolated receptors (4, 26, 36). Such interactions will impact on both iGluR location and conformation in response to agonist binding. We propose that the concept illustrated here, where small molecule and protein ligands cooperate in order to modulate GluD2 signaling, is likely to be more generally applicable to neurotransmitter receptors.

Supplementary Material

Refer to Web version on PubMed Central for supplementary material.

Acknowledgments

GluD2$_{ATD}$, GluD1$_{ATD}$ and Cbln1$_{C1q}$–GluD2$_{ATD}$ are deposited in the Protein Data Bank (PDB codes 5KC5, 5KC6, 5KC7, 5KC8, 5KC9 and 5KCA, respectively).

References

1. Traynelis SF, et al. Glutamate receptor ion channels: structure, regulation, and function. Pharmacological reviews. 2010; 62:405–496. DOI: 10.1124/pr.109.002451 [PubMed: 20716669]

2. Karakas E, Furukawa H. Crystal structure of a heterotetrameric NMDA receptor ion channel. Science. 2014; 344:992–997. DOI: 10.1126/science.1251915 [PubMed: 24876489]

3. Lee CH, et al. NMDA receptor structures reveal subunit arrangement and pore architecture. Nature. 2014; 511:191–197. DOI: 10.1038/nature13548 [PubMed: 25008524]

4. Nakagawa T, Cheng Y, Ramm E, Sheng M, Walz T. Structure and different conformational states of native AMPA receptor complexes. Nature. 2005; 433:545–549. DOI: 10.1038/nature03328 [PubMed: 15690046]

5. Sobolevsky AI, Rosconi MP, Gouaux E. X-ray structure, symmetry and mechanism of an AMPA-subtype glutamate receptor. Nature. 2009; 462:745–756. DOI: 10.1038/nature08624 [PubMed: 19946266]

6. Herguedas B, et al. Structure and organization of heteromeric AMPA-type glutamate receptors. Science. 2016; doi: 10.1126/science.aad3873

7. Kakegawa W, Kohda K, Yuzaki M. The delta2 'ionotropic' glutamate receptor functions as a non-ionotropic receptor to control cerebellar synaptic plasticity. The Journal of physiology. 2007; 584:89–96. DOI: 10.1113/jphysiol.2007.141291 [PubMed: 17702810]

8. Kakegawa W, et al. D-Serine regulates cerebellar LTD and motor coordination through the delta 2 glutamate receptor. Nat Neurosci. 2011; 14:603–U693. DOI: 10.1038/Nn.2791 [PubMed: 21460832]

9. Kohda K, et al. The delta2 glutamate receptor gates long-term depression by coordinating interactions between two AMPA receptor phosphorylation sites. Proc Natl Acad Sci U S A. 2013; 110:E948–957. DOI: 10.1073/pnas.1218380110 [PubMed: 23431139]

10. Aow J, Dore K, Malinow R. Conformational signaling required for synaptic plasticity by the NMDA receptor complex. Proc Natl Acad Sci U S A. 2015; 112:14711–14716. DOI: 10.1073/pnas.1520029112 [PubMed: 26553983]

11. Dore K, Aow J, Malinow R. Agonist binding to the NMDA receptor drives movement of its cytoplasmic domain without ion flow. Proc Natl Acad Sci U S A. 2015; 112:14705–14710. DOI: 10.1073/pnas.1520023112 [PubMed: 26553997]

12. Weilinger NL, et al. Metabotropic NMDA receptor signaling couples Src family kinases to pannexin-1 during excitotoxicity. Nat Neurosci. 2016; 19:432–442. DOI: 10.1038/nn.4236 [PubMed: 26854804]

13. Auger C, Ogden D. AMPA receptor activation controls type I metabotropic glutamate receptor signalling via a tyrosine kinase at parallel fibre-Purkinje cell synapses. The Journal of physiology. 2010; 588:3063–3074. DOI: 10.1113/jphysiol.2010.191080 [PubMed: 20603338]

14. Hayashi T, Umemori H, Mishina M, Yamamoto T. The AMPA receptor interacts with and signals through the protein tyrosine kinase Lyn. Nature. 1999; 397:72–76. DOI: 10.1038/16269 [PubMed: 9892356]

15. Rodrigues RJ, Lerma J. Metabotropic signaling by kainate receptors. WIREs Membr Transp Signal. 2012; 1:399–410. DOI: 10.1002/wmts.35

16. Matsuda K, et al. Cbln1 is a ligand for an orphan glutamate receptor delta2, a bidirectional synapse organizer. Science. 2010; 328:363–368. DOI: 10.1126/science.1185152 [PubMed: 20395510]

17. Sia GM, et al. Interaction of the N-terminal domain of the AMPA receptor GluR4 subunit with the neuronal pentraxin NP1 mediates GluR4 synaptic recruitment. Neuron. 2007; 55:87–102. DOI: 10.1016/j.neuron.2007.06.020 [PubMed: 17610819]

18. Uemura T, et al. Trans-synaptic interaction of GluRdelta2 and Neurexin through Cbln1 mediates synapse formation in the cerebellum. Cell. 2010; 141:1068–1079. DOI: 10.1016/j.cell.2010.04.035 [PubMed: 20537373]

19. Saglietti L, et al. Extracellular interactions between GluR2 and N-cadherin in spine regulation. Neuron. 2007; 54:461–477. DOI: 10.1016/j.neuron.2007.04.012 [PubMed: 17481398]

20. Matsuda K, et al. Transsynaptic Modulation of Kainate Receptor Functions by C1q-like Proteins. Neuron. 2016; 90:752–767. DOI: 10.1016/j.neuron.2016.04.001 [PubMed: 27133466]

21. Hirai H, et al. Cbln1 is essential for synaptic integrity and plasticity in the cerebellum. Nat Neurosci. 2005; 8:1534–1541. DOI: 10.1038/nn1576 [PubMed: 16234806]

22. Ryu K, Yokoyama M, Yamashita M, Hirano T. Induction of excitatory and inhibitory presynaptic differentiation by GluD1. Biochemical and biophysical research communications. 2012; 417:157–161. DOI: 10.1016/j.bbrc.2011.11.075 [PubMed: 22138648]

23. Yasumura M, et al. Glutamate receptor delta1 induces preferentially inhibitory presynaptic differentiation of cortical neurons by interacting with neurexins through cerebellin precursor protein subtypes. Journal of neurochemistry. 2012; 121:705–716. DOI: 10.1111/j. 1471-4159.2011.07631.x [PubMed: 22191730]

24. Materials and methods are available as supplementary materials on *Science* Online

25. Bao D, Pang Z, Morgan JI. The structure and proteolytic processing of Cbln1 complexes. Journal of neurochemistry. 2005; 95:618–629. DOI: 10.1111/j.1471-4159.2005.03385.x [PubMed: 16135095]

26. Meyerson JR, et al. Structural mechanism of glutamate receptor activation and desensitization. Nature. 2014; 514:328–334. DOI: 10.1038/nature13603 [PubMed: 25119039]

27. Clayton A, et al. Crystal structure of the GluR2 amino-terminal domain provides insights into the architecture and assembly of ionotropic glutamate receptors. Journal of molecular biology. 2009; 392:1125–1132. DOI: 10.1016/j.jmb.2009.07.082 [PubMed: 19651138]

28. Jin R, et al. Crystal structure and association behaviour of the GluR2 amino-terminal domain. The EMBO journal. 2009; 28:1812–1823. DOI: 10.1038/emboj.2009.140 [PubMed: 19461580]

29. Kumar J, Schuck P, Jin R, Mayer ML. The N-terminal domain of GluR6-subtype glutamate receptor ion channels. Nature structural & molecular biology. 2009; 16:631–638. DOI: 10.1038/nsmb.1613

30. Koehnke J, et al. Splice Form Dependence of beta-Neurexin/Neuroligin Binding Interactions. Neuron. 2010; 67:61–74. DOI: 10.1016/J.Neuron.2010.06.001 [PubMed: 20624592]

31. Kashiwabuchi N, et al. Impairment of motor coordination, Purkinje cell synapse formation, and cerebellar long-term depression in GluR delta 2 mutant mice. Cell. 1995; 81:245–252. [PubMed: 7736576]

32. Naur P, et al. Ionotropic glutamate-like receptor delta2 binds D-serine and glycine. Proc Natl Acad Sci U S A. 2007; 104:14116–14121. DOI: 10.1073/pnas.0703718104 [PubMed: 17715062]

33. Ito M, Yamaguchi K, Nagao S, Yamazaki T. Long-term depression as a model of cerebellar plasticity. Progress in brain research. 2014; 210:1–30. DOI: 10.1016/B978-0-444-63356-9.00001-7 [PubMed: 24916287]

34. Kakegawa W, et al. Differential regulation of synaptic plasticity and cerebellar motor learning by the C-terminal PDZ-binding motif of GluRdelta2. J Neurosci. 2008; 28:1460–1468. DOI: 10.1523/JNEUROSCI.2553-07.2008 [PubMed: 18256267]

35. Ito-Ishida A, et al. Presynaptically released Cbln1 induces dynamic axonal structural changes by interacting with GluD2 during cerebellar synapse formation. Neuron. 2012; 76:549–564. DOI: 10.1016/j.neuron.2012.07.027 [PubMed: 23141067]

36. Dürr KL, et al. Structure and dynamics of AMPA receptor GluA2 in resting, pre-open, and desensitized states. Cell. 2014; 158:778–792. DOI: 10.1016/j.cell.2014.07.023 [PubMed: 25109876]

37. Yelshanskaya MV, Li M, Sobolevsky AI. Structure of an agonist-bound ionotropic glutamate receptor. Science. 2014; 345:1070–1074. DOI: 10.1126/science.1256508 [PubMed: 25103407]

One Sentence Summary

A molecular bridge across excitatory synapses provides a structural framework that facilitates signaling in the cerebellum.
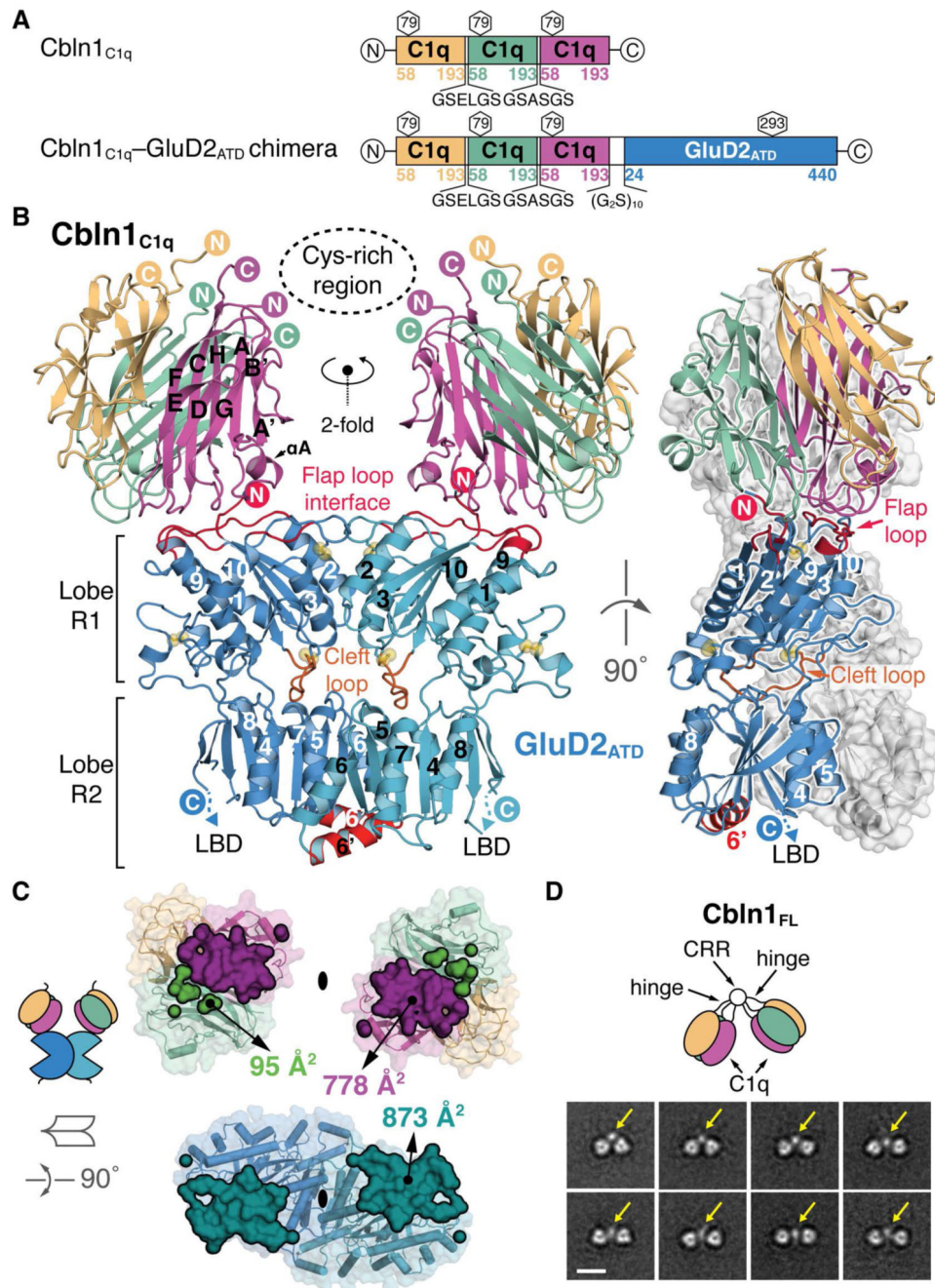
Fig. 1. Architecture of the Cbln1$_{C1q}$–GluD2$_{ATD}$ Binary Complex.
(**A**) Schematic representation of the chimeric Cbln1$_{C1q}$ and Cbln1$_{C1q}$–GluD2$_{ATD}$ constructs.
(**B**) "Front" and "side" view of the Cbln1$_{C1q}$–GluD2$_{ATD}$ complex. The inward tilted
orientation of the Cbln1 C1q domains suggests the position of the Cbln1 cysteine-rich region
(CRR), as visible in EM class averages and represented by a dotted ellipse here. GluD2 α-
helix 6' and flap and cleft loops are highlighted. Disulfide bridges are shown as yellow
spheres. (**C**) Symmetry-breaking in the Cbln1$_{C1q}$ interface. The total buried interaction
surface is shown in a 90° rotated open book view. (**D**) Selected negative-stain EM class

averages of Cbln1$_{FL}$ illustrate its dimer-of-trimers arrangement. Yellow arrows indicate the suggested position of the CRR that links both C1q trimers. Scale bar: 10 nm.
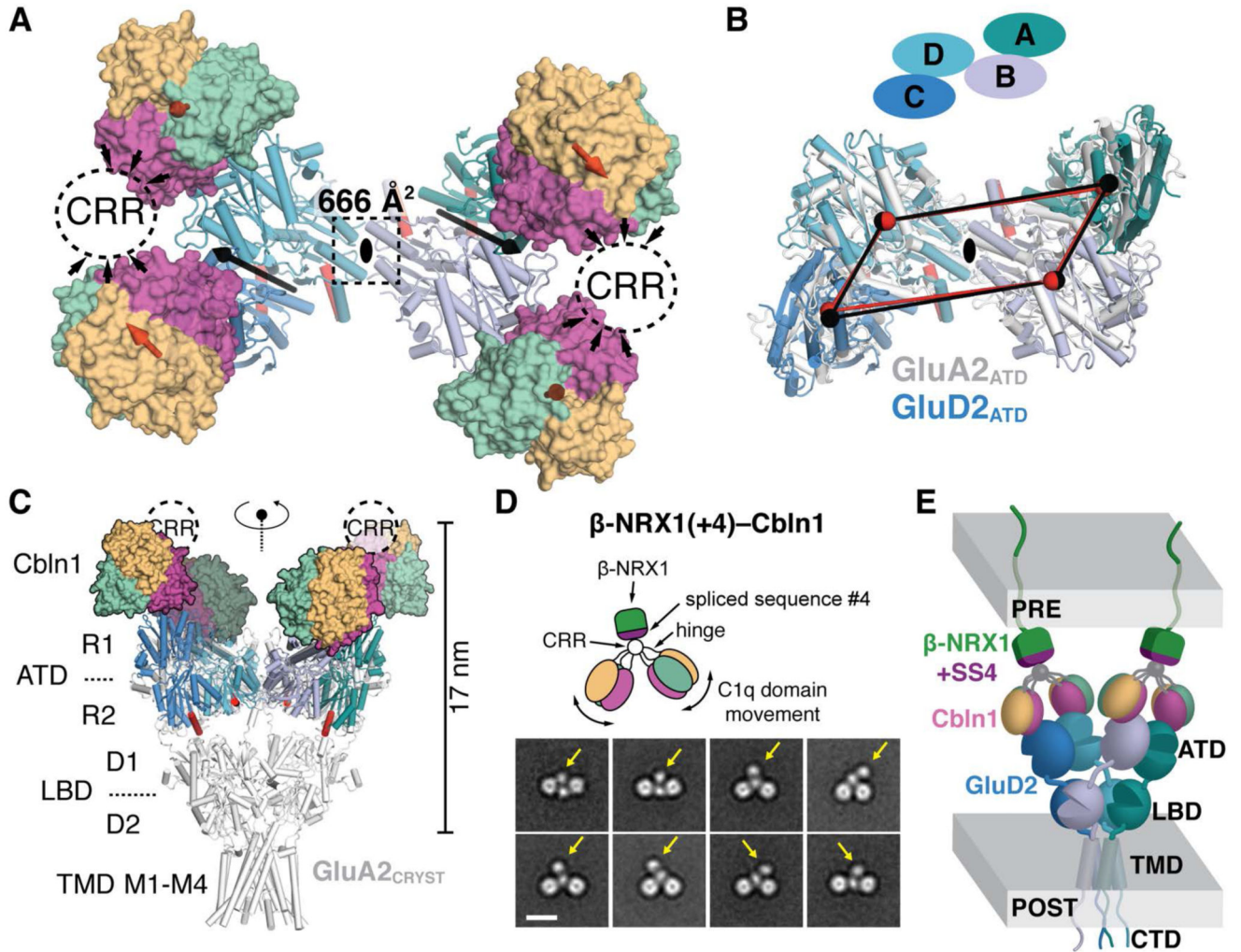
Fig. 2. Quaternary Structure of the β-NRX1–Cbln1–GluD2 Complex.
(**A**) "Top" view of the full $Cbln1_{C1q}$–$GluD2_{ATD}$ dimer-of-dimers complex. The black ellipse, black arrows and red arrows indicate the overall two-fold symmetry axis, the two-fold symmetry axes in the $GluD2_{ATD}$ dimers and the three-fold symmetry axes in the $Cbln1_{C1q}$ trimers, respectively. The suggested position of the Cbln1 CRR is marked with dashed ovals. (**B**) Superposition of the GluD2 and GluA2 (PDB 3KG2, (5)) N-shaped ATD layers using the B–D ATD dimers (view equivalent to (A)). Centers of mass of $GluD2_{ATD}$ (black spheres) and $GluA2_{ATD}$ (red spheres) are connected to highlight overall similarity. (**C**) View along the overall two-fold axis of the $Cbln1_{C1q}$–$GluD2_{ATD}$ complex aligned to Y-shaped $GluA2_{CRYST}$ using the B–D ATD dimers. (**D**) Selected negative-stain EM class averages of the β-NRX1(+4)–$Cbln1_{FL}$ complex. Yellow arrows indicate the suggested position of β-NRX1(+4). Scale bar; 10 nm. CRR; cysteine-rich region. (**E**) Model of the synapse-spanning β-NRX1(+4)–Cbln1–GluD2 complex.
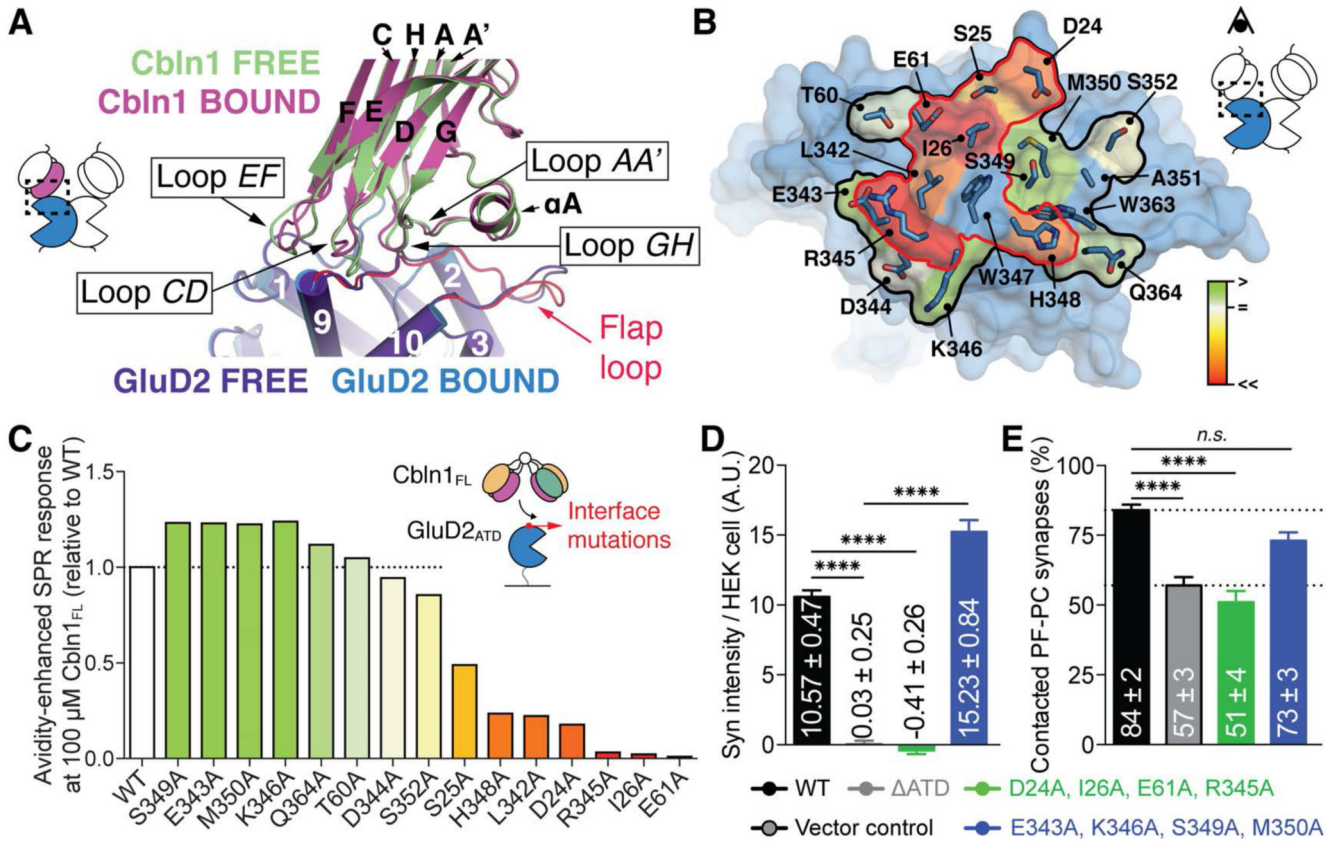
Fig. 3. Details and Structure-guided Mutagenesis of the Cbln1–GluD2 Interface.
(**A**) Superposition of free and bound $Cbln1_{C1q}$ and $GluD2_{ATD}$. (**B**) GluD2 alanine-scanning mutagenesis; SPR response levels are color-annotated as a heat map onto the GluD2 ATD structure. The mutated interface is outlined in black, and the interaction hotspot is outlined in red. (**C**) GluD2 alanine-scanning mutagenesis using $Cbln1_{FL}$ and monomerised $GluD2_{ATD}$. The bar chart shows absolute SPR responses after stimulation with 100 μM Cbln1, relative to wild-type GluD2. (**D**) Quantification of hemi-synapse formation by cerebellar granule cells (GCs) and HEK 293T cells expressing structure-guided GluD2 mutants. Syn; synaptophysin. Data represent mean ± SEM. ****; $p < 0.0001$ (Kruskal-Wallis and Steel-Dwass test). (**E**) Quantification of contacted synapses between PFs and PCs expressing structure-guided GluD2 mutants in *Grid2*-null (GluD2-deficient) cerebella. Data represent mean ± SEM. ****; $p < 0.0001$, *n.s.*; not significant (Kruskal-Wallis and Steel-Dwass test).
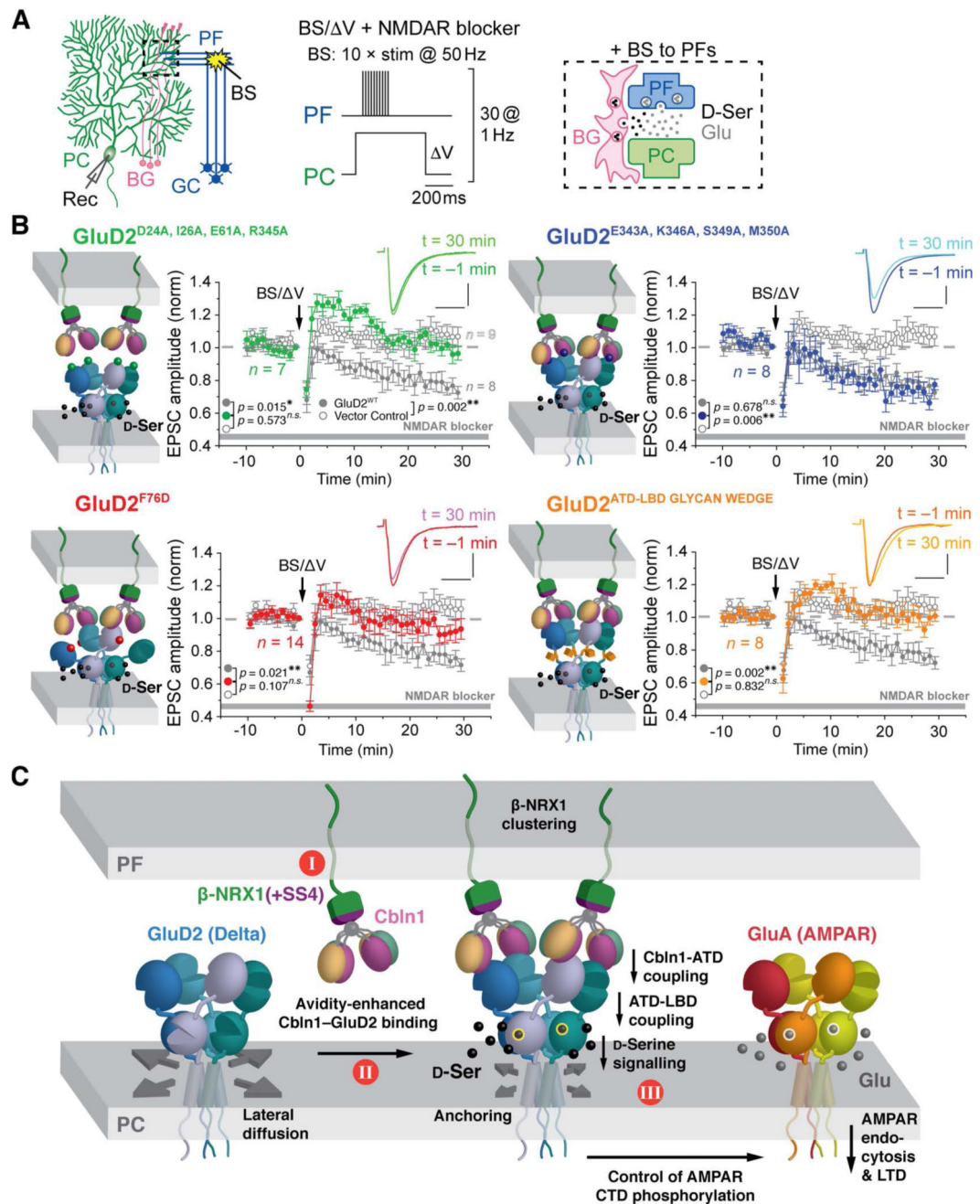
Fig. 4. Structure-guided GluD2 Mutants Affect Cerebellar Synaptic Plasticity.
(**A**) Setup to induce LTD in immature PC dendrites. PC: Purkinje cell, GC: granule cell, PF: parallel fiber, BG: Bergmann glia, BS: burst stimulation, Rec: recording electrode. (**B**) Averaged LTD data from immature *Grid2*-null (GluD2-deficient) PCs expressing GFP + GluD2 variants, after burst PF stimulation (BS) combined with direct PC depolarization (ΔV) (BS/ΔV; arrow). The insets show PF-EPSCs at t = −1 min and t = 30 min time points relative to BS/ΔV application. Data represent the mean ± SEM. **; $p < 0.01$, *; $p < 0.05$, *n.s.*; not significant (Kruskal-Wallis and Steel-Dwass test). NMDA receptor blockers are 100

μM D-AP5 plus 25 μM MK801. **(C)** Proposed key events leading to signal transmission in the β-NRX1(+4)–Cbln1– GluD2 triad. I; β-NRX1–Cbln1 is a pre-synaptic anchor for GluD2. II; trans-synaptic complex formation. GluD2 allows binding of two β-NRX1(+4)–Cbln1 complexes and is shown at full occupancy. III; GluD2, Cbln1 and D-Ser cooperatively induce postsynaptic LTD.